

# Advanced dispersion engineering of a III-Nitride micro-resonator for a blue/UV frequency comb

Ali Eshaghian Dorche<sup>\*1,2</sup>, Doğan Timuçin<sup>†2</sup>, Krishnan Thyagarajan<sup>2</sup>,  
Thomas Wunderer<sup>2</sup>, Noble Johnson<sup>2</sup>, and David Schwartz<sup>2</sup>

<sup>1</sup>*School of Electrical and Computer Engineering, Georgia Institute of Technology,  
777 Atlantic Drive NW, Atlanta, GA 30332, USA*

<sup>2</sup>*Palo Alto Research Center (PARC), A Xerox Company,  
3333 Coyote Hill Road, Palo Alto, CA 94304, USA*

June 16, 2020

## Abstract

A systematic dispersion engineering approach is presented toward designing a III-Nitride micro-resonator for a blue/UV frequency comb. The motivation for this endeavor is to fill the need for compact, coherent, multi-wavelength photon sources that can be paired with, *e.g.*, the  $^{171}\text{Yb}^+$  ion in a photonic integrated chip for optical sensing, time-keeping, and quantum computing applications. The challenge is to overcome the normal material dispersion exhibited by the otherwise ideal (*i.e.*, low-loss and large-Kerr-coefficient) AlGaIn family of materials, as this is a prerequisite for bright-soliton Kerr comb generation. The proposed approach exploits the avoided-crossing phenomenon in coupled waveguides to achieve strong anomalous dispersion in a desired wavelength range. The resulting designs reveal a wide range of dispersion response tunability, and are realizable with the current state-of-the-art growth and fabrication methods for AlGaIn semiconductors. Numerical simulations of the spatio-temporal evolution of the intracavity field under continuous-wave laser pumping indicate that such a structure is capable of generating a broadband blue/UV bright-soliton Kerr frequency comb.

---

<sup>\*</sup>This work was performed while A. E. D. was a 2019 summer intern at PARC.

<sup>†</sup>Corresponding author contact: [dtimucin@parc.com](mailto:dtimucin@parc.com)

# 1 Introduction

Frequency standards play an important role both in fundamental science and in a wide range of applications such as sensing, metrology, and position, navigation & timing, to name just a few. The field was revolutionized by the advent of the optical frequency comb [1]. Over the past decade, integrated photonic approaches to optical frequency comb generation have received much attention as a potential technology for enabling ultra-precise measurements in a miniaturized platform [2, 3], wherein the generation of stable, coherent frequency components (also called comb lines) is achieved through the injection of a continuous-wave (CW) laser into a micro-resonator exhibiting third-order (*i.e.*, Kerr) nonlinearity [4, 5]. A dissipative Kerr soliton provides a tool for generating coherent and low-noise comb lines over a wide spectral range, circumventing the challenges associated with sub-comb processes in non-solitonic Kerr combs, which suffer from much higher noise.

There has been significant progress on both theoretical and experimental fronts, to the point where we now have fully developed spectro- and spatio-temporal models [6, 7] of the nonlinear dynamical Kerr-comb generation process inside a micro-resonator, advanced dispersion engineering approaches [8–11] for micro-resonator design optimization, as well as fabrication processes for Si<sub>3</sub>N<sub>4</sub>-based structures [12–14], allowing the manufacture of near-IR micro-resonators with very high quality factors ( $Q$ ) in a variety of material platforms (Si, SiO<sub>2</sub>, Si<sub>3</sub>N<sub>4</sub>, SiC, diamond, AlN, AlGaAs, GaP, MgF<sub>2</sub>). These advances have enabled the laboratory demonstrations of frequency-bin entangled photon sources and Doppler-cooling of atoms/ions [15, 16], among others.

While there has been extensive reporting on efficient bright-soliton Kerr-comb generation at mid-infrared, and more recently at near-visible, wavelengths as highlighted above, there has been no report of direct Kerr-comb generation in the blue and UV end of the spectrum. This is largely due to the significant normal dispersion exhibited by candidate materials that otherwise have desirable features such as large bandgaps and reasonably strong third-order nonlinearity at these wavelengths. Indeed, ternary and quaternary III-V semiconductors, and specifically the group III-N materials, are very promising for ultrashort pulse generation at short wavelengths, but are unfortunately normally dispersive.

Anomalous dispersion is a favorable, if not essential, ingredient for generating broadband bright-soliton Kerr combs. This is because soliton formation is greatly aided by the anomalous dispersion of the cold (unloaded) cavity, which can compensate for the (normal) Kerr-nonlinearity dispersion

of the loaded resonator. Purely geometric approaches to achieving anomalous dispersion typically lead to feature sizes that are impractical to fabricate in the blue/UV wavelength regime, therefore necessitating a more advanced dispersion engineering approach.

In this paper, we describe a systematic dispersion engineering approach for achieving anomalous dispersion in an AlGaIn micro-resonator at blue/UV wavelengths. At the core of the approach is the avoided-crossing behavior exhibited by coupled waveguides, which we use to our advantage in designing a hybrid structure that is at once reasonably easy to fabricate and highly tailorable in its dispersion response. Similar ideas have been used before at visible and near-IR wavelengths, working with Si or Si<sub>3</sub>N<sub>4</sub> where  $Q$  can be very high [17–19]; the added challenge here is to achieve anomalous dispersion in a micro-resonator with a moderate  $Q$ . We then describe an AlGaIn heterostructure that embodies these dispersion engineering principles toward the demonstration of a Kerr comb with our micro-resonator design.

The utility of an AlGaIn-based blue/UV frequency comb design is evidenced by the recent interest in optical timing, trapping, and quantum computing applications employing Ytterbium, which has a number of suitable optical transitions; see Figure 1. The application of AlN for optical waveguides and micro-resonators has been explored recently [21, 22]. Pumped by a quantum-well UV/visible laser grown and fabricated on a common nitride epitaxial wafer [23], a micro-resonator generating a broadband Kerr comb would be an ideal integrated photonic source for such applications.

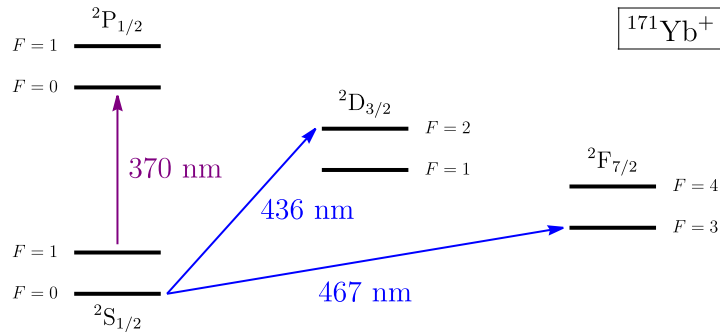


Figure 1: Energy diagram for the  $^{171}\text{Yb}^+$  ion (adapted from [20]), showing the blue and UV transitions germane to our discussion: 436 nm and 467 nm optical clock transitions (blue arrows) and 370 nm Doppler-cooling transition (purple arrow).

## 2 Proposed method

An individual waveguide mode with a propagation constant  $\beta(\omega)$  has a group velocity  $1/v_g = d\beta/d\omega \equiv \beta'(\omega)$ , whose (frequency) dispersion is, in turn, given by  $d^2\beta/d\omega^2 \equiv \beta''(\omega)$ . The two group velocity dispersion (GVD) regimes are delineated by the sign of this latter quantity; *i.e.*,  $\beta'' > 0$  for normal, and  $\beta'' < 0$  for anomalous. The III-Nitride materials exhibit strong normal dispersion in the blue/UV part of the spectrum, and therefore are not inherently suitable for bright-soliton generation.

Consider instead *two* waveguides with intrinsic propagation constants  $\beta_1$  and  $\beta_2$  that exhibit coherent, evanescent, co-directional coupling. The mutual coupling strengths  $\kappa_{12}$  and  $\kappa_{21} = \kappa_{12}^*$  can be tailored by adjusting the thickness of the gap between the guides. It is well known (see, *e.g.*, [24], §8.2) that such a hybrid structure possesses a pair of super-modes with propagation constants

$$\beta_{\pm} = \bar{\beta} \pm \sqrt{\Delta\beta^2 + \kappa^2}, \quad (1)$$

where  $\kappa = \sqrt{\kappa_{12}\kappa_{21}} = |\kappa_{12}|$ , and we defined

$$\bar{\beta} = \frac{1}{2}(\beta_1 + \beta_2), \quad (2)$$

$$\Delta\beta = \frac{1}{2}(\beta_1 - \beta_2). \quad (3)$$

These super-modes are further distinguished by their symmetric (+) and anti-symmetric (−) spatial field profiles over the transverse cross-section of the hybrid structure.

Now, let  $\omega_c$  denote the central frequency around which we wish to engineer anomalous dispersion in the hybrid structure. The geometric parameters of the high-index layers are then designed to achieve phase matching between the two guides at this frequency; *i.e.*,

$$\beta_1(\omega_c) = \beta_2(\omega_c). \quad (4)$$

The propagation constants  $\beta_{\pm}(\omega)$  of the *hybrid guide* display the so-called “avoided crossing” (also known as “level repulsion”) behavior around  $\omega_c$ . This effect, controlled through the coupling parameter  $\kappa$ , makes it possible to push  $\beta''_{-}$  toward negative values, thus suppressing the normal material dispersion and achieving a net anomalous dispersion in the odd super-mode of the hetero-structure.

In order to explore this possibility in detail, we differentiate (1) with respect to  $\omega$  to obtain

$$\begin{aligned}\beta'_{\pm} &= \bar{\beta}' \pm \frac{\Delta\beta \Delta\beta' + \kappa \kappa'}{\sqrt{\Delta\beta^2 + \kappa^2}}, \\ \beta''_{\pm} &= \bar{\beta}'' \mp \frac{(\Delta\beta \Delta\beta' + \kappa \kappa')^2}{(\Delta\beta^2 + \kappa^2)^{3/2}} \pm \frac{(\Delta\beta')^2 + \Delta\beta \Delta\beta'' + (\kappa')^2 + \kappa \kappa''}{\sqrt{\Delta\beta^2 + \kappa^2}}.\end{aligned}\quad (5)$$

Evaluating these expressions at  $\omega = \omega_c$  by making use of (3) and (4), we find

$$\begin{aligned}\beta'_{\pm}(\omega_c) &= \bar{\beta}'(\omega_c) \pm \kappa'(\omega_c), \\ \beta''_{\pm}(\omega_c) &= \bar{\beta}''(\omega_c) \pm \left\{ \frac{[\Delta\beta'(\omega_c)]^2}{\kappa(\omega_c)} + \kappa''(\omega_c) \right\}.\end{aligned}\quad (6)$$

The first term on the right-hand side of (6) is positive, since the individual guides are assumed at the outset to have normal dispersion. Fortunately, however, the first term in the curly braces is also strictly positive, and if it can be made sufficiently large by a judicious choice of material and geometric parameters, then the whole right-hand side of (6) can be made to go negative for (and only for) the odd super-mode, thus rendering it anomalously dispersive, as desired. This effect persists over a band of frequencies around  $\omega_c$ , beyond which the guides become phase-mismatched and the dispersion behavior reverts to the normal regime.

### 3 Dispersion engineering

We now choose a basic hybrid waveguide structure to demonstrate the approach proposed above. We exclusively focus on the odd super-mode, and drop the subscript on  $\beta_-$ . Defining an effective refractive index through  $\beta = (\omega/c) n_{\text{eff}}$ , the GVD parameter of this super-mode will be computed via

$$D_{\lambda} = -\frac{\lambda}{c} \frac{d^2 n_{\text{eff}}}{d\lambda^2},$$

where  $c$  is the vacuum speed of light, and we switched to the customary wavelength variable  $\lambda = 2\pi c/\omega$ , which makes it more convenient to work with refractive-index data for optical materials. The anomalous dispersion behavior will now be indicated by  $D_{\lambda} > 0$ .

Figure 2(a) shows a vertical stack of two rectangular waveguides with heights  $h_{f1}$  and  $h_{f2}$  and a common width  $w$ , separated by a gap of height

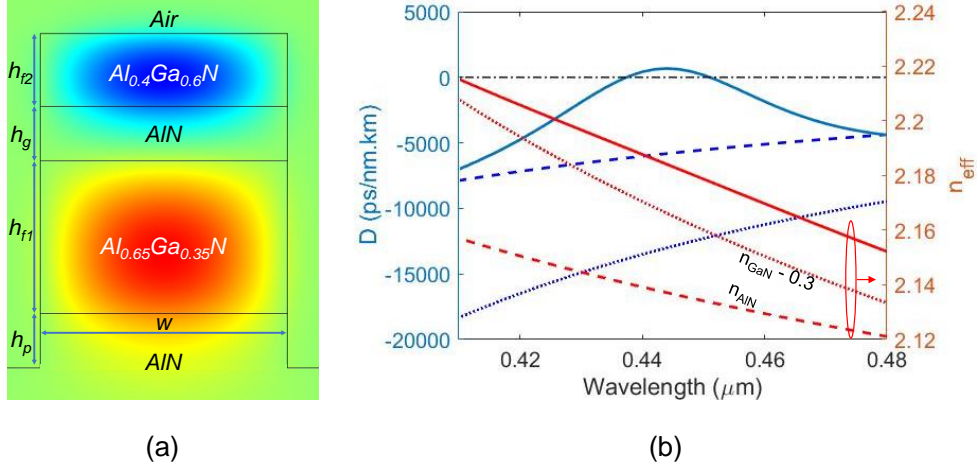


Figure 2: (a) A representative AlGaIn hybrid waveguide structure and the intensity profile of its fundamental odd super-mode at  $\lambda = 442$  nm. The dimensions are  $h_p = 150$  nm,  $h_{f1} = 440$  nm,  $h_g = 250$  nm,  $h_{f2} = 200$  nm, and  $w = 700$  nm. The Al mole fractions are  $x_1 = 0.65$  and  $x_2 = 0.4$ . (b) The GVD parameter  $D_\lambda$  (solid blue) and the effective refractive index  $n_{\text{eff}}$  (solid red) of the odd super-mode as functions of wavelength near the avoided-crossing point. The dashed and dotted curves show the GVD parameters (blue) and the (ordinary) refractive indices (red) for *bulk* AlN and GaN, respectively (data from [25]; the index of bulk GaN is shifted down by 0.3 for plotting purposes).

$h_g$  and sitting on a pedestal of height  $h_p$ . The two guides are made of  $\text{Al}_x\text{Ga}_{1-x}\text{N}$  (with  $x_1 \neq x_2$ , in general), whereas the gap and the pedestal are made of AlN. The waveguide heterostructure is shown on an AlN substrate with no (dielectric) encapsulation.

We studied the eigenmodes of this structure numerically using the Wave Optics Module of the finite-element modeling software COMSOL Multiphysics. With consideration of the blue/UV transitions of the  $^{171}\text{Yb}^+$  ion in mind and guided by the analytical results of the previous section, we selected the geometric parameters and the material compositions of the structure such that the avoided-crossing wavelength falls around 442 nm. As shown in Fig. 2, the fundamental odd super-mode at this wavelength has an anti-symmetric transverse field profile, as expected, which is a perturbed superposition (with a phase shift of  $\pi$  rad) of the two quasi-TE ( $\text{HE}_{00}$ ) modes of the individual rectangular guides. The figure caption lists the parameters of this particular structure, which are readily achievable via standard

epitaxial growth techniques.

Figure 2(b) shows the GVD parameter as well as the effective refractive index of the odd super-mode. As the figure reveals, both AlN and GaN are normally dispersive at these wavelengths, and yet, this particular design of the hybrid structure is able to achieve anomalous dispersion near the target wavelength interval, as indicated by the portion of the blue curve for which  $D_\lambda$  goes positive.

We next assessed the sensitivity of the GVD parameter to the key geometric parameters of the hybrid structure, namely, its width, the gap height, and heights of the individual guides. The results of this study are summarized in Figure 3, where the curves with dots indicate the GVD profile of the optimal design shown in Figure 2; *i.e.*, they are the same as the solid blue  $D_\lambda$  curve shown in Fig. 2(b).

Deviations of the waveguide width  $w$  from its target value can arise from imprecise etching of the epitaxial layers. Accordingly, we investigated a representative range of  $\pm 20$  nm around the nominal design value of 700 nm. As can be seen in Fig. 3(a), this has an imperceptible impact on  $D_\lambda$ , which is not surprising since  $w$  is appreciably larger than  $\lambda$  in all three cases.

Deviations from target values of the height parameters can be expected to be negligible, since the epitaxial layer thickness is usually a well-controlled parameter at the level of a few monolayers of resolution. This fact notwithstanding, even small deviations from an optimal design value in the vertical direction may be expected to significantly impact the GVD parameter of the resulting hybrid structure, since this is the direction along which crucial coupling takes place. With this in mind, we investigated a modest  $\pm 5$  nm range of variation around the target values of  $h_{f1}$ ,  $h_{f2}$ , and  $h_g$ . As can be seen in Figs. 3(b) and 3(d), increasing  $h_{f1}$  results in a gradual shifting of the  $D_\lambda$  peak up and to the left (in wavelength), while increasing  $h_{f2}$  shifts the  $D_\lambda$  peak much more dramatically and in the opposite direction (down and to the right). The reason for this is the considerable difference in the slopes of the dispersion curves  $\beta_1$  and  $\beta_2$  near the avoided-crossing point, which are, in turn, controlled by the aspect ratios of the individual guides [24]. Finally, an increase in  $h_g$  causes little change in the position of the peak but does enhance the value of  $D_\lambda$  significantly, as seen in Fig. 3(c). This can be understood from our results in the previous section, as follows. The coupling coefficient  $\kappa$  is given approximately by an overlap integral between the modes of the individual guides [24]. Consequently, a larger  $h_g$  translates into a smaller  $\kappa$ , which, in turn, makes the second term in (6) larger, with the overall effect of driving  $\beta''$  more negative.

As mentioned before, the run-to-run processing variability in these geo-

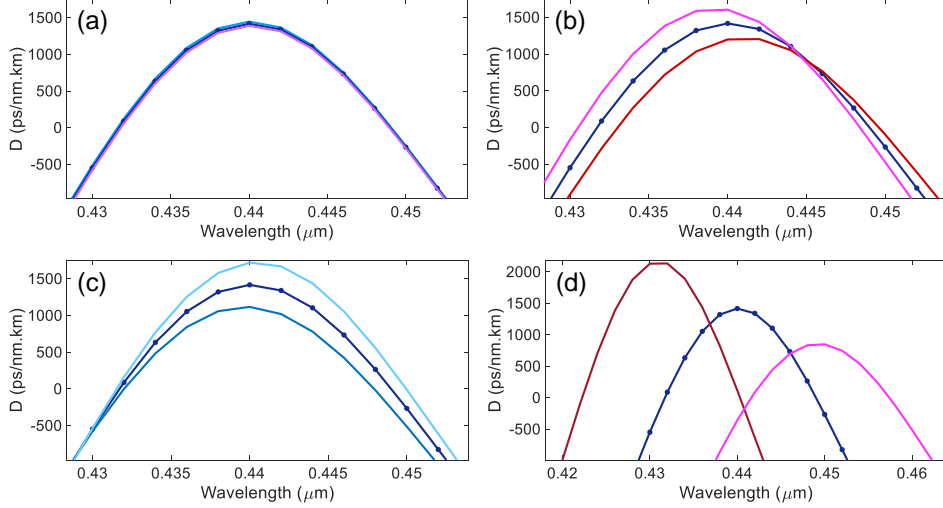


Figure 3: Sensitivity of the GVD parameter  $D_\lambda$  to the geometric parameters of the hybrid structure shown in Fig. 2. The violet curves with dots correspond to the optimal (underlined) design values. (a) Guide width  $w = 680$  (blue), 700, and 720 nm (magenta). (b) Guide 1 height  $h_{f1} = 435$  (brown), 440, and 445 nm (magenta). (c) Gap height  $h_g = 245$  (blue), 250, and 255 nm (cyan). (d) Guide 2 height  $h_{f2} = 195$  (brown), 200, and 205 nm (magenta).

metric parameters is likely to be smaller than the  $\pm 5$  nm range considered here. The observed sensitivity is therefore more relevant as a demonstration of the range of tunability of the anomalous dispersion response. By suitably optimizing the thicknesses of the high-index regions as well as the thickness of the gap, it should be possible to increase or decrease the peak  $D_\lambda$  value while shifting the positive- $D_\lambda$  band toward shorter or longer wavelengths, thus tailoring the anomalous dispersion response of the structure as desired.

## 4 Comb generation

With anomalous dispersion in the blue/UV part of the spectrum achievable in a III-Nitride material system through advanced dispersion engineering as described in the previous section, we are motivated to investigate the formation of a Kerr cavity soliton in a microring resonator with radius  $R$

and transverse cross-section as shown in Fig. 2. Closing the waveguide upon itself in this manner results in a (countably infinite) set of cavity modes whose resonant frequencies satisfy  $2\pi R\beta(\omega) = 2\pi l$ ; *i.e.*, they are given by

$$\omega_l = \zeta\left(\frac{l}{R}\right) \quad (7)$$

for positive integer  $l$ , where  $\zeta(\cdot) = \beta^{-1}(\cdot)$ .\*

Assume now that the resonator is pumped by a continuous-wave (CW) laser with frequency  $\omega_0$  that is near a cavity resonance at  $\omega_\ell$ . Let  $\phi$  denote the (azimuthal) coordinate around the resonator, and transform to a frame that is rotating with the group velocity (at  $\omega_\ell$ ) in the cavity by defining  $\theta = \phi - (v_g/R)t$ . The spatio-temporal evolution<sup>†</sup> of the normalized intra-cavity mode amplitude  $\psi(\theta, t)$  is then found to be governed by the Lugiato–Lefever equation (LLE) [7]

$$\frac{\partial\psi}{\partial t} = -(1 + i\tilde{\delta})\psi + i|\psi|^2\psi - i\frac{\tilde{\beta}}{2}\frac{\partial^2\psi}{\partial\theta^2} + F, \quad (8)$$

where  $F$  is the normalized pump amplitude in the cavity,  $\tilde{\delta}$  is proportional to the detuning  $\delta = \omega_0 - \omega_\ell$  of the pump frequency from the nearest cold-cavity resonance, and  $\tilde{\beta}$  is proportional to the GVD parameter  $\beta''$  and therefore indicates the nature and the strength of dispersion in the cavity. The LLE is a driven nonlinear Schrödinger equation with damping<sup>‡</sup> and detuning, and therefore soliton formation may be expected for  $\tilde{\beta} < 0$ .

In addition to anomalous dispersion, another important consideration for Kerr comb generation is the competition between four-wave mixing gain and Raman gain. The former is the very mechanism that leads to comb formation while the latter tends to be stronger, and therefore it is crucial to ensure their separation in the frequency domain. For a laser wavelength of  $\lambda_0 = 442$  nm,

---

\*It should perhaps be mentioned that one must apply a “curvature” correction (of order  $w/R$ ) to  $\beta(\omega)$  of the linear waveguide in order to obtain the corresponding propagation constant of the circular waveguide. [It is this latter function that enters into (7) and (8)]. For the geometric parameters chosen here, this is indeed a small correction; however, it should be accounted for when considering the optimal placement of a linear waveguide section for coupling into and out of the circular resonator.

<sup>†</sup>This is essentially a mean-field approximation to the more rigorous coupled-mode approach [6]. The latter provides an alternative spectro-temporal description of the process, which is quite a bit more costly to model computationally.

<sup>‡</sup>Cavity losses include (small) material absorption, radiation loss that is exacerbated by the bending of the guide, and (small) transmittance of the coupling port. An overall damping coefficient  $\alpha$  does not appear explicitly in (8), however, since it is aggregated with other terms during the normalization process.

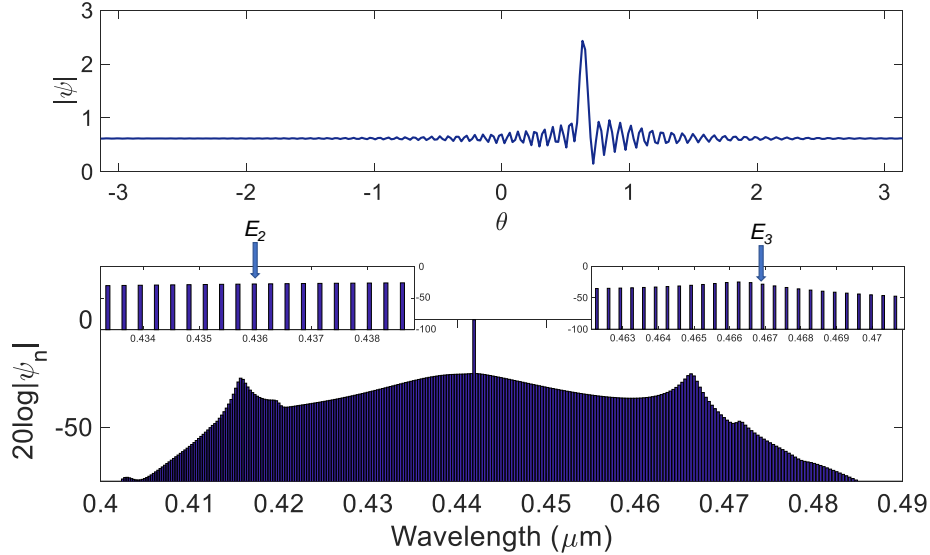


Figure 4: Intra-cavity Kerr soliton (top) and associated normalized frequency-comb spectrum (bottom) in a microring resonator with radius  $R = 40 \mu\text{m}$  and transverse cross-section shown in Fig. 2, driven by a CW laser at  $\lambda_0 = 442 \text{ nm}$ . The two insets highlight the specific comb lines matching the  $^{171}\text{Yb}^+$  ion optical clock transitions at  $436 \text{ nm}$  ( $E_2$ ) and  $467 \text{ nm}$  ( $E_3$ ), respectively.

the anti-Stokes lines in crystalline AlGaIn are separated by about 18 THz from the pump frequency, with a linewidth of about 100 GHz [26]. By choosing the ring radius to be  $R = 40 \mu\text{m}$ , we place the free spectral range of the resonator at about 400 GHz, thus minimizing the overlap between the Raman gain spectrum and the cavity modes.

With a normalized detuning of  $\tilde{\delta} = 3.5$  and a normalized pump power of  $F^2 = 3.85$ , the numerical solution of (8) via the standard split-step Fourier method [27] yields the bright Kerr soliton and the corresponding frequency-comb spectrum shown in Figure 4. As can be seen, the comb spans a wide spectral range in excess of 75 nm at the  $-70 \text{ dB}$  window, thus providing strong comb lines at the optical clock transitions  $E_2$  and  $E_3$  of  $^{171}\text{Yb}^+$ .

## 5 Conclusion

In this paper, our goal was to leverage the state-of-the-art photonic materials and fabrication techniques toward designing an integrated optical frequency

combs in the UV and short-wavelength-visible regions of the spectrum. With the relevant transitions of the  $^{171}\text{Yb}^+$  ion targeted for concreteness in the design exercise reported here, we demonstrated the design of an anomalously dispersive hybrid micro-resonator structure using III-Nitride family materials that exhibit normal dispersion in this spectral regime. The design approach exploits the avoided-crossing phenomenon in coupled waveguides, and leads to practicably realizable resonator dimensions while allowing for a wide range of tunability of the dispersion response. Numerical solutions of the Lugiato–Lefever equation demonstrated the capability of the designed micro-resonator to support the formation of a broadband Kerr-soliton blue/UV frequency comb under CW pumping.

## References

- [1] T. W. Hänsch, “Nobel lecture: Passion for precision,” *Rev. Mod. Phys.* **78**, 1297–1309 (2006).
- [2] P. Del’Haye, A. Schliesser, O. Arcizet, T. Wilken, R. Holzwarth, and T. J. Kippenberg, “Optical frequency comb generation from a monolithic micro-resonator,” *Nature* **450**, 1214–1217 (2007).
- [3] T. J. Kippenberg, R. Holzwarth, and S. A. Diddams, “Microresonator-based optical frequency combs,” *Science* **332**, 555–559 (2011).
- [4] S. A. Diddams, “The evolving optical frequency comb,” *J. Opt. Soc. Am. B* **27**, B51–B62 (2010).
- [5] Y. K. Chembo, “Kerr optical frequency combs: theory, applications and perspectives,” *Nanophotonics* **5**, 214–230 (2016).
- [6] Y. K. Chembo and N. Yu, “Modal expansion approach to optical-frequency-comb generation with monolithic whispering-gallery-mode resonators,” *Phys. Rev. A* **82**, 033801 (2010).
- [7] Y. K. Chembo and C. R. Menyuk, “Spatiotemporal Lugiato-Lefever formalism for Kerr-comb generation in whispering-gallery-mode resonators,” *Phys. Rev. A* **87**, 053852 (2013).
- [8] A. E. Dorche, S. Abdollahramezani, H. Taheri, A. A. Eftekhar, and A. Adibi, “Extending chip-based Kerr-comb to visible spectrum by dispersive wave engineering,” *Opt. Express* **25**, 22362–22374 (2017).

- [9] A. E. Dorche, A. H. Hosseinnia, A. A. Eftekhar, and A. Adibi, “Wide-band bright-soliton frequency-comb generation at optical telecommunication wavelength in a thin silicon nitride film,” *Journal of Nanophotonics* **12**, 046008 (2018).
- [10] A. E. Dorche, A. A. Eftekhar, and A. Adibi, “Near-visible bright-soliton Kerr comb generation in dispersion-engineered lithium niobate coupled optical micro-resonators,” *CLEO/QELS-Fundamental Science, JTh2A-55* (2019).
- [11] S. Kim, K. Han, C. Wang, J. A. Jaramillo-Villegas, X. Xue, C. Bao, Y. Xuan, D. E. Leaird, A. M. Weiner, and M. Qi, “Dispersion engineering and frequency comb generation in thin silicon nitride concentric micro-resonators,” *Nature Communications* **8**, 372 (2017).
- [12] X. Ji, F. A. Barbosa, S. P. Roberts, A. Dutt, J. Cardenas, Y. Okawachi, A. Bryant, A. L. Gaeta, and M. Lipson, “Ultra-low-loss on-chip resonators with sub-milliwatt parametric oscillation threshold,” *Optica* **4**, 619–624 (2017).
- [13] M. H. P. Pfeiffer, C. Herkommer, J. Liu, T. Morais, M. Zervas, M. Geiselmann, and T. J. Kippenberg, “Photonic Damascene process for low-loss, high-confinement silicon nitride waveguides,” *IEEE Journal of Selected Topics in Quantum Electronics* **24**, 1–11 (2018).
- [14] Y. Xuan, Y. Liu, L. T. Varghese, A. J. Metcalf, X. Xue, P. H. Wang, K. Han, J. A. Jaramillo-Villegas, A. A. Noman, C. Wang, and S. Kim, “High-Q silicon nitride micro-resonators exhibiting low-power frequency comb initiation,” *Optica* **3**, 1171–1180 (2016).
- [15] C. Reimer, M. Kues, P. Roztocky, B. Wetzels, F. Grazioso, B. E. Little, S. T. Chu, T. Johnston, Y. Bromberg, L. Caspani, D. J. Moss, and R. Morandotti, “Generation of multiphoton entangled quantum states by means of integrated frequency combs,” *Science* **351**, 1176–1180 (2016).
- [16] N. Šantić, D. Buhin, D. Kovačić, I. Krešić, D. Aumiler, and T. Ban, “Cooling of atoms using an optical frequency comb,” *Scientific reports* **9**, 2510 (2019).
- [17] L. Zhang, Y. Yue, R. G. Beausoleil, and A. E. Willner, “Flattened dispersion in silicon slot waveguides,” *Opt. Express* **18**, 20529–20534 (2010).

- [18] L. Zhang, Y. Yue, Y. Xiao-Li, J. Wang, R. G. Beausoleil, and A. E. Willner, “Flat and low dispersion in highly nonlinear slot waveguides,” *Opt. Express* **18**, 13187–13193 (2010).
- [19] Y. Guo, Z. Jafari, A. M. Agarwal, L. C. Kimerling, G. Li, J. Michel, and L. Zhang, “Bilayer dispersion-flattened waveguides with four zero-dispersion wavelengths,” *Opt. Lett.* **41**, 4939–4942 (2016).
- [20] S. V. Chepurov, A. A. Lugovoy, S. N. Kuznetsov, K. M. Rumynin, M. V. Okhapkin, A. V. Taichenachev, V. I. Yudin, and S. N. Bagayev, “Optical frequency standard with ytterbium single ion,” *Journal of Physics: Conf. Series* **793**, 012004 (2017).
- [21] T.-J. Lu, M. Fanto, H. Choi, P. Thomas, J. Steidle, S. Mouradian, W. Kong, D. Zhu, H. Moon, K. Berggren, J. Kim, M. Soltani, S. Preble, and D. Englund, “Aluminum nitride integrated photonics platform for the ultraviolet to visible spectrum,” *Opt. Express* **26**, 11147–11160 (2018).
- [22] X. Liu, A. W. Bruch, Z. Gong, Juanjuan Lu, J. B. Surya, L. Zhang, J. Wang, J. Yan, and H. X. Tang, “Ultra-high- $Q$  UV microring resonators based on a single-crystalline AlN platform,” *Optica* **5**, 1279–1282 (2018).
- [23] T. Wunderer, C. L. Chua, J. E. Northrup, Z. Yang, N. M. Johnson, M. Kneissl, G. A. Garrett, H. Shen, M. Wraback, B. Moody, H. S. Craft, R. Schlessler, R. F. Dalmau, and Z. Sitar, “Optically pumped UV lasers grown on bulk AlN substrates,” *physica status solidi* **9**, 1–4 (2012).
- [24] S. L. Chuang, *Physics of Photonic Devices* (2<sup>nd</sup> ed.), Wiley, Hoboken, NJ (2009).
- [25] M. Soltani, R. Soref, T. Palacios, and D. Englund, “AlGaIn/AlN integrated photonics platform for the ultraviolet and visible spectral range,” *Opt. Express* **24**, 25415–25423 (2016).
- [26] H. Jung, Z. Gong, X. Liu, X. Guo, C.-L. Zuo, and H. X. Tang, “Stokes and anti-Stokes Raman scatterings from frequency comb lines in polycrystalline aluminum nitride microring resonators,” *Opt. Express* **27**, 22246–22253 (2019).
- [27] J. A. C. Weideman and B. M. Herbst, “Split-step methods for the solution of the nonlinear Schrödinger equation,” *SIAM J. Numer. Anal.* **23**, 485–507 (1986).